Tunneling between edge states in the quantum Hall regime limited by a mesoscopic island: A current-plateau phenomenon

Z. H. Liu, G. Nachtwei, J. Groß, R. R. Gerhardts, J. Weis, K. von Klitzing, and K. Eberl

Max-Planck-Institut für Festkörperforschung, Heisenbergstraße 1, D-70569 Stuttgart, Germany

Well-developed current plateaus have been observed in the *I-V* characteristics of Corbino devices in the quantum Hall regime, if a striplike island of mesoscopic dimensions is located between two trench fingers which are etched radially between the central and outer Ohmic contacts. The trenches are 100 nm wide and define, together with the island, two constrictions of 550–700-nm width. The current plateaus are due to a limitation of the tunneling rate by the filling of nonequilibrium states around the island. The evolution of the current plateaus with the filling factor is qualitatively explained by quasielastic inter-Landau-level tunneling. The latter mechanism determines the onset of the tunneling-current plateau, which extends until the complete local breakdown of the quantum Hall regime around the island is reached. We investigated this tunneling phenomenon as a function of the temperature in the range from 23 mK to 2.1 K, and for various sizes of the island, ranging from 100×250 nm^2 to 100 nm$\times 8$ μm. The plateaus were better pronounced, the lower the temperature and the smaller the island was. To explain the observed tunneling-current plateaus, we suggest a picture including the properties of the edge states (near the trenches and around the island) and the incompressible quantum Hall region in between them. [S0163-1829(98)04731-6]

I. INTRODUCTION

In two-dimensional electron systems (2DES) with lateral confinement, edge channels form near the boundaries in quantizing magnetic fields.[1] These edge channels can dominate the electronic transport[2] and provide a possible explanation for the quantum Hall effect (QHE),[3,4] and a variety of related phenomena (for an overview, see Ref. 5). Therefore, tunneling between edge states was extensively investigated both theoretically and experimentally (see also Ref. 5).

Recently, tunneling between edge states of a device which contains an antidot in the middle of a mesoscopic constriction was investigated.[6–8] At very low excitations, Aharonov-Bohm (AB) oscillations were observable in the conductivity.[6–8]

We have patterned a similar structure on a Corbino device, and investigated the current-voltage characteristics in the QH regime. No tunneling current was observable at small source-drain voltages. This is due to the formation of incompressible regions (insulating barriers) between the compressible edge states near the trenches and around the island in between at integer filling factors.[9] At higher voltages, we observed well-developed current steps in the *I-V* characteristics of such an arrangement, which we attribute to a limitation of the tunneling current by the charging of nonequilibrium states around the island.

The main differences of our study from the experiments of Refs. 6–8 on similar constrictions are the size of the object in between the two trenches (longer in our case) and the mode of operation, which works far from equilibrium by the application of high local electric fields instead of aiming on the AB effect. To realize this mode of operation, the constriction had to be wide enough to provide a stable QH current path at lower voltages, but small enough to allow tunneling at higher voltages. Thus the tunneling is effectively suppressed up to rather large source-drain voltages, and the onset of current flow is far beyond the range where the AB effect is observable.

II. SAMPLES

All devices were fabricated from two Ga$_{1-x}$Al$_x$As/GaAs heterostructures containing a 2DES, with different densities n_s and mobilities μ_H ($n_s = 2.2 \times 10^{11}$ cm^{-2}, $\mu_H = 8.0 \times 10^5$ cm^2/V s for sample I; and $n_s = 3.1 \times 10^{11}$ cm^{-2}, $\mu_H = 1.3 \times 10^5$ cm^2/V s for the three samples of sample set II). Figure 1 shows the scheme of the device: in a Corbino ring with a channel width of 75 μm, two trench fingers with a width of about 100 nm in the narrowest region are etched radially between the central and outer Ohmic contacts, defining a small constriction with widths of 1.5 μm (sample I), 1.2 μm (samples IIa and IIc), and 2.1 μm (sample IIb). An oval antidot with a size of 100×300 nm^2 (sample I) is etched in the center of the constriction, with the long direction perpendicular to the trench fingers (Fig. 1). The island of the samples of set II have a width of 100 nm and variable lengths of 250 nm (sample IIa), 1 μm (sample IIb), and 8 μm (sample IIc), oriented either along (sample IIb) or perpendicular (samples IIa and IIc) to the trench finger direction. The whole pattern was prepared by electron-beam lithography, followed by reactive ion etching. The etching was performed to a depth of about 100 nm to ensure a complete removing of the 2DES (the Si doping layer was located at 60 nm below the cap layer) in the pattern region. In the QH regime, this arrangement represents a tunneling device: the compressible strips surrounding the two trench fingers, being either in contact with the central or outer Ohmic contacts of the Corbino ring, form the source and the drain contact. The island provides electronic states which are isolated from the
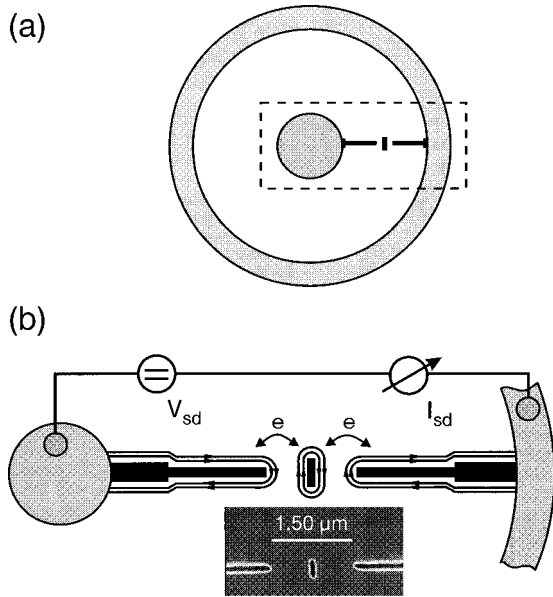
FIG. 1. (a) Scheme of the device: two trench fingers and an antidot (black regions) are etched between the central Ohmic contact and outer Ohmic contact (grey regions) of a Corbino ring. (b) Enlarged view of the part in the dashed line box marked in (a). Compressible edge strips at $\nu=2$ and the measurement setup are shown. Below: scanning electron microscope image of the pattern (sample I).

source and the drain contact by incompressible regions, and are capable of storing electronic charges. The Corbino geometry allows for a direct measurement of the tunneling current between the source and the drain contact.

III. EXPERIMENTS

The dc I-V measurements were performed in a ^{3}He-^{4}He dilution refrigerator with a base temperature of 23 mK (sample I), and in a conventional ^{4}He cryostat with temperatures down to 1.3 K (samples of set II). All samples were briefly illuminated with a red light-emitting diode at the temperature of $T=1.3$ K, increasing the electron density to $n_s = 2.6 \times 10^{11}$ cm^{-2} (sample I) and $n_s = (3.7-4.0) \times 10^{11}$ cm^{-2} (samples of set II). The increased carrier density was found to be persistent during the measurements, which were performed in the dark. The illumination is essential for an appropriate adjustment of the confinement potential near the sample boundaries, as explained in Sec. IV of this paper. Figure 2(a) shows the I-V characteristic of sample I at $\nu = 2$ ($B = 5.35$ T) and $T = 23$ mK, where $\nu = n_s h / eB$ is the filling factor. The trace exhibits well-developed current steps, with $|V_{sd}|$ onset values between 30 and 40 mV, and with current step heights $|\Delta I|$ between 3.0 and 4.0 nA. The trace [Fig. 2(a)] did not depend on the sweep rate, and no obvious hysteresis was observed in both sweep directions. In Fig. 2(b), the I-V characteristics of sample IIa, measured at $\nu = 2$ ($B = 8.20$ T) and $T = 1.3$ K, show a current step at $V_{sd} \approx -33$ mV with a step height ΔI of about -3.7 nA. A slight hysteresis is visible at larger $|V_{sd}|$ voltages [Fig. 2(b)]. A pronounced asymmetry of the I-V characteristics, in particular concerning the shape of the current plateaus, is observable with respect to the current polarity [Figs. 2(a) and 2(b)]. We attribute this asymmetry, which was found even more
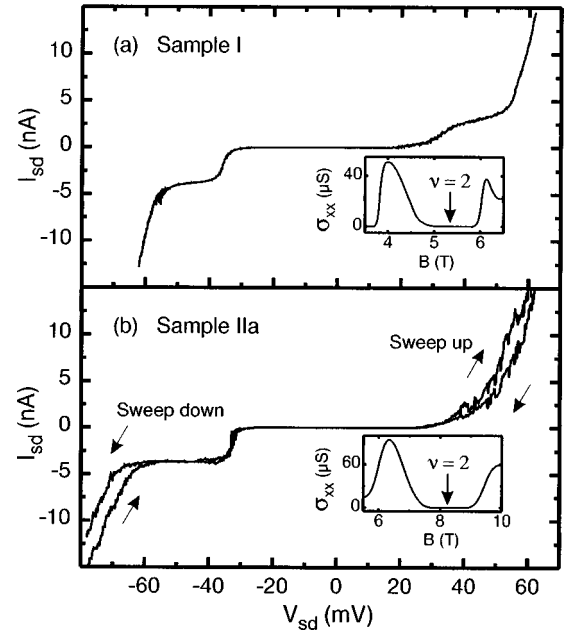
FIG. 2. I-V characteristics of the Corbino samples at $\nu=2$: (a) sample I ($T=23$ mK, $B=5.35$ T); (b) sample IIa ($T=1.3$ K, $B=8.20$ T). Insets: Shubnikov–de Haas curves for the samples around $\nu=2$.

pronounced in all samples of set II [Figs. 2(b) and 6] to asymmetric tunneling barriers, which are typical in such a mesoscopic system.

In contrast to the formation of current plateaus in samples with a constriction and an island, for the reference samples (i.e., Corbino rings without constriction on the same chip as sample II), an abrupt onset of the QHE breakdown at $\nu=2$ occurs at a much higher $|V_{sd}|$ [in the range between 500 and 600 mV; see Fig. 3(a)]. We did not observe current plateaus
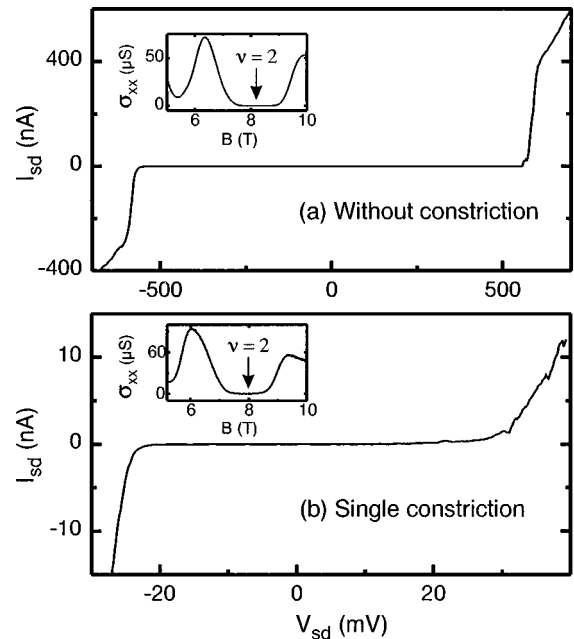
FIG. 3. I-V characteristics at $\nu=2$ of reference Corbino samples on the same chip as sample set II, measured at $T=1.3$ K: (a) unpatterned Corbino sample with channel width of 75 μm ($B=8.18$ T); (b) Corbino sample with a single constriction of 550 nm width ($B=8.0$ T). Insets: Shubnikov–de Haas curves for the samples around $\nu=2$.
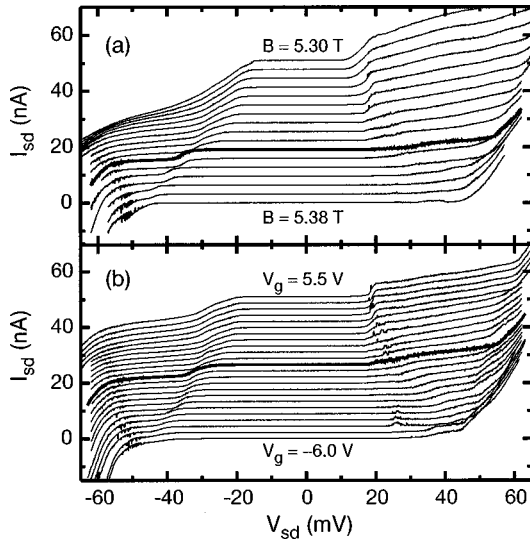
FIG. 4. Evolution of the I-V characteristics of sample I near $\nu=2$ ($T=23$ mK): (a) with magnetic field B (steps 5 mT, back-gate voltage $V_g=0$). Thick curve: $B=5.35$ T, i.e., $\nu=2$. (b) With back-gate voltage V_g (step 0.5 V; $B=5.35$ T kept fixed). Thick curve: $V_g=0$, i.e., $\nu=2$. For clarity, the traces in (a) and (b) are plotted with a vertical offset.

FIG. 5. The current step's onset V_{sd}^{on} (a) and the absolute current step height $|\Delta I|$ (b) as a function of $\Delta\nu/\nu$. The data points are analyzed from the current steps in the negative V_{sd} side in Fig. 4 (a) (solid squares, $\Delta\nu/\nu=-\Delta B/B$) and in Fig. 4(b) (open circles, $\Delta\nu/\nu=(h/\nu e^2 B)\cdot c_{bg}\Delta V_g$). The circles fit well with the squares, yielding $c_{bg}\approx 4.0\times10^{-7}$ F/m^2.

for samples with a single constriction of different widths but without the antidot island. In Fig. 3(b), a typical I-V characteristic of samples with a single constriction of 550-nm width is shown. The breakdown was found at $|V_{sd}|$ values of about 20–30 mV, and no current plateau was observable. The sudden current onset in these samples is due to a local breakdown of the QHE. The comparison of the I-V characteristics of our three sample types (Corbino device without constriction, with a single constriction only and with a constriction and an island) gives evidence that the source-drain current onset of our patterned devices originates from a breakdown of the QHE close to the constriction. Interestingly, an apparently similar sudden onset of source-drain current in the I-V characteristic was observed in the tunneling across a submicron trench in a 2DES at zero magnetic field.[10] However, the similarities concern only the appearance of the effect, as the experiments by Pilling et al. were explained by a sudden onset of charge transfer via a deeper 2D layer due to field emission under a permanent illumination.[10] In our case, the onset of current flow near the constriction of the Corbino samples is due to the nonequilibrium population of higher Landau levels.[11–13] We attribute the observed current plateaus in the corresponding devices to a limitation of the tunneling current by the electron states around the island, which act as a ''bottleneck'' for the electronic transport.

In Fig. 4, the evolution of the I-V characteristics of sample I with either magnetic field or the back-gate voltage clearly shows that it is the bulk filling factor of the incompressible regions in between the antidot and the trench fingers which define the barrier properties of our tunneling devices. A slight decrease of the filling factor by increasing the magnetic field according to $\Delta\nu=-\nu\Delta B/B$, or by decreasing the back-gate voltage according to $\Delta\nu=(h/e^2B)c_{bg}\Delta V_g$ ($c_{bg}\approx 4.0\times10^{-7}$ F/m^2 is the capacitance per unit area between the back-gate and the 2DES), leads to higher $|V_{sd}|$ onsets and smaller step height values $|\Delta I|$, respectively, as shown in Figs. 4 and 5. A reduction of the filling factor by less than 0.6%, corresponding to an increase of magnetic field from 5.35 to 5.38 T [Fig. 4(a)], or to applying a back-gate voltage of -6.0 V [Fig. 4(b)], results in a complete disappearance of the current steps. The evolution of the I-V characteristics with the filling factor or the magnetic field, respectively, behave qualitatively similarly for the samples of sample set II, as shown in Fig. 6. The three sets of curves correspond to three different sizes and orientations of the island inside the constriction, as depicted in the insets of Figs. 6(a)–6(c). For all samples, the current onset shifts to higher $|V_{sd}|$ values with increasing magnetic field (decreasing filling factor). The presence of the current plateau within a very narrow range of filling factors (1.5%–2.5%), which is typically a factor of 10 smaller than the QH plateau width, is also common for all samples. As clearly visible in particular from the evolution of the curves of Fig. 6(a), the filling factor range, where current plateaus occur, includes the integer value and values slightly above. This means that the local Fermi energy of the incompressible QH state between the trenches and the island lies in the middle or slightly above the middle between two Landau levels. Also common for all samples is the $|V_{sd}|$ range, in which current steps occur (a current onset between about 25 and 40 mV, and a complete breakdown between about 55 and 65 mV). This is remarkable in view of the very different island sizes and orientations of the samples. The only common parameter of all samples is the constriction width of 2×550 nm^2, which obviously determines the complete breakdown at $|V_{sd}|\approx 60$ mV (in accordance with the breakdown at a single constriction of 550-nm width for $|V_{sd}|\approx 20$–30 mV). The relation of the current step onset to the sample parameters is far more complicated, and will be discussed below. The height of the current step, $|\Delta I|$, was found between 3 and 5 nA for the small islands 100×300 nm^2 or 100×250 nm^2 for samples I and IIa, and between 6 and 8 nA for the larger islands 100 nm$\times(1$–$8)$ μm for samples IIb and IIc. There is a clear trend that the flatter the plateaus, the smaller the island and the higher the magnetic field (in the middle of the $\nu=2$ QH plateau). In particular, sample IIa, with the smallest island and the highest electron density, shows a completely flat current plateau with a constant tunneling current of -3.7 nA over a $|V_{sd}|$
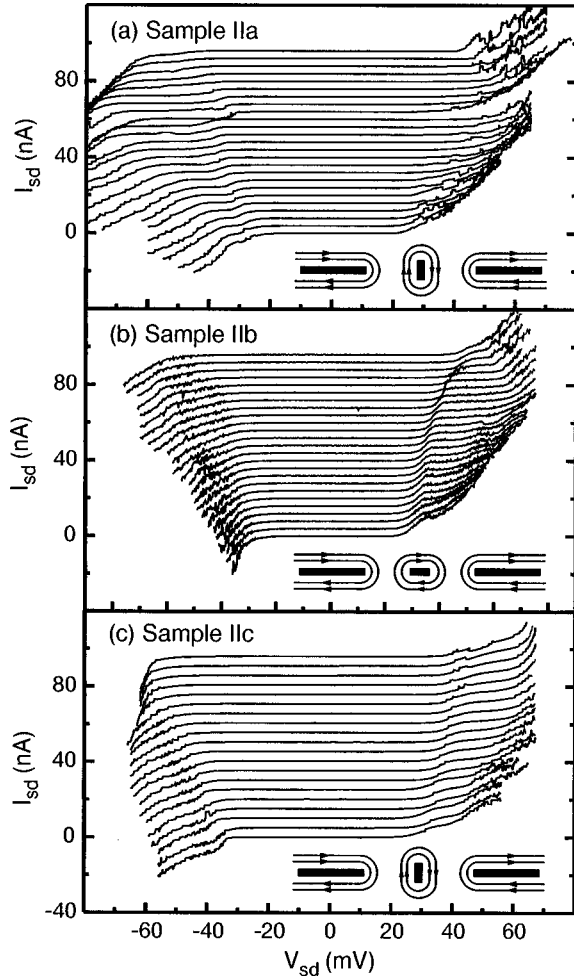
FIG. 6. Evolution of the I-V characteristics of sample set II near $\nu=2$ with magnetic field B at $T=1.3$ K: (a) sample IIa; (b) sample IIb; (c) sample IIc. For the traces from bottom to top, B varies from 8.04 to 8.28 T (10-mT steps) in (a); from 7.46 to 7.58 T (5-mT steps) in (b); and from 7.58 to 7.77 T (10-mT steps) in (c). For clarity the traces in (a), (b), and (c) are plotted with a vertical offset. The current step onsets occur at V_{sd} values between -25 and -40 mV in (a), and between 25 and 40 mV in (b) and (c), with step heights ΔI between -3 and -5 nA in (a) and between 6 and 8 nA in (b) and (c). Three insets indicate the island geometry. The islands are of 100-nm width, with lengths of 250 nm in (a), 1 μm in (b), and 8 μm in (c).

range of about 20 mV [see the curves in Fig. 2(b)]. We will return to this point later.

To obtain a deeper insight into the physical nature of the current steps observed, we have investigated their temperature dependence. For sample I, the I-V characteristics at a fixed magnetic field of $B=5.31$ T [the range of magnetic field where the current step occurs (see Fig. 4) was shifted about 40 mT to the lower magnetic field side after the second measurement cycle between 23 mK and 1.4 K] are shown in Fig. 7(a) for different temperatures in the range 23 mK$\leqslant T \leqslant 1.4$ K. Obviously, the current step becomes smoother, the onset shifts to lower $|V_{sd}|$ values, and the step height $|\Delta I|$ increases with temperature. The same tendency applies for sample IIb, as visible from the plots in Fig. 7(b) ($T=1.8$ K) and (c) ($T=2.1$ K). Moreover, the filling factor range, in which current steps occur, shrinks from 1.8% at $T=1.3$ K to about 0.5% at $T=2.1$ K. As visible from the inset of Fig.
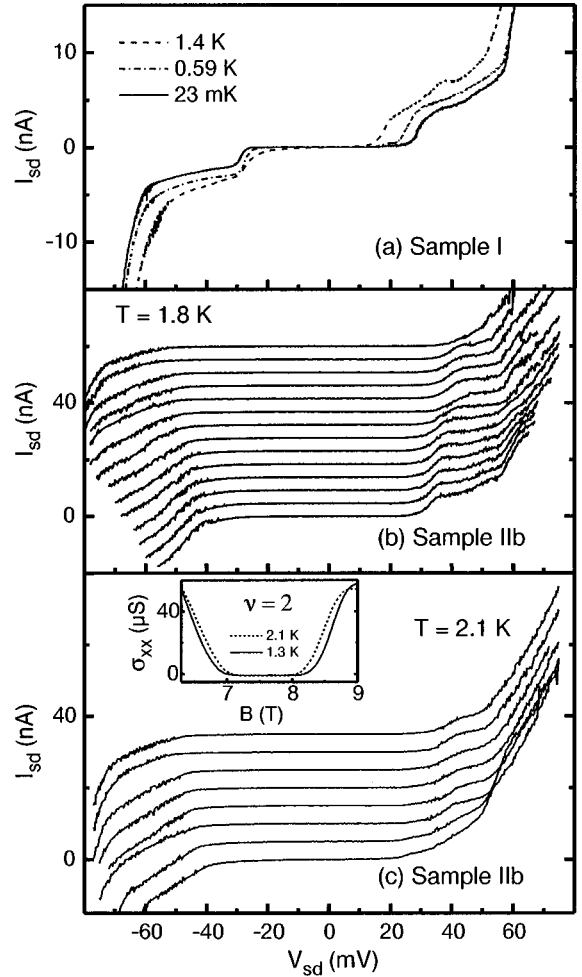
FIG. 7. (a) I-V characteristics of sample I at $B=5.31$ T ($\nu=2$) for temperatures of 23 mK, 0.59 K, and 1.4 K. In (b) and (c), I-V characteristics of sample IIb at temperatures of $T=1.8$ K and 2.1 K are shown. For clarity, the traces in (b) and (c) are plotted with a vertical offset. For traces from bottom to top, the magnetic field B varies from 7.410 to 7.475 T (5-mT steps) in (b), and from 7.410 to 7.445 T (5-mT steps) in (c). Inset in (c): Shubnikov–de Haas curves of sample IIb near $\nu=2$ at temperatures of 1.3 and 2.1 K.

7(c), the width of the QH plateau is far less reduced by the same change of temperature. As the current steps also occur only in a filling factor range which is only one-tenth of the QH plateau width, the observed tunneling effect is apparently far more sensitive to external parameters than the QHE itself.

IV. CONCLUSIONS

The evolution of the current steps with the filling factor suggests that the source-drain current onset is induced by the quasielastic tunneling between Landau levels [so-called quasielastic inter-Landau-level scattering (QUILLS), see Ref. 11]. According to this model, tunneling of electrons from the highest occupied LL into the lowest empty LL can be induced by a large Hall field, causing the onset of the QHE breakdown. In Corbino devices, the source-drain voltage is equivalent to the Hall voltage. The QUILLS process predicts a critical electric field of the QHE breakdown $F_{cr} \propto \hbar\omega_c/el_B \propto B^{3/2}$ [$\hbar\omega_c$ is the Landau gap, and l_B
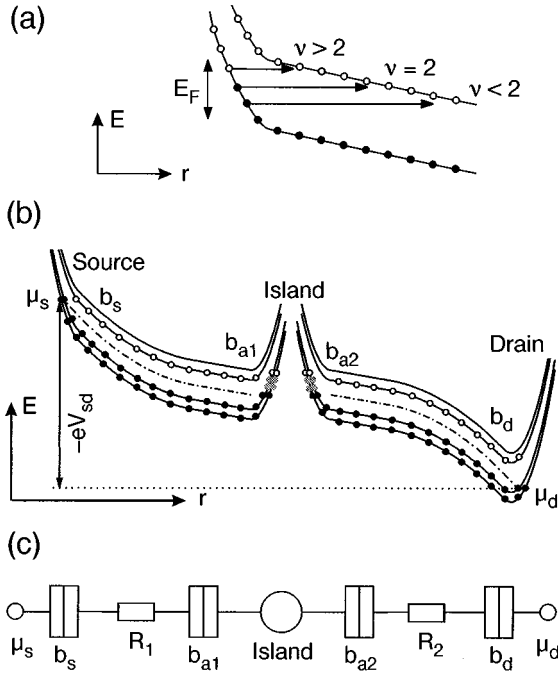
FIG. 8. (a) Decrease of the filling factor near $\nu=2$, causing a wider effective tunneling barrier for a typical QUILLS at the local Fermi level is illustrated. Spin splitting is neglected. (b) Scheme of the LL bending in the constriction between source and drain at a finite V_{sd}, with μ_s and μ_d the chemical potentials of the source and drain. The dash-dotted line represents the local Fermi energy. Solid circles represent occupied states in an $n=0$ spin-split LL, and open circles represent empty states in the $n=0$ and 1 spin-split LL. Grey circles at the island represent the additional electrons occupying the electron states around the antidot. (c) Proposed equivalent electric circuit of the system, with b_s, b_{a1}, b_{a2}, and b_d for the four QUILLS barriers, and with R_1 and R_2 for the effective resistances for the excited electrons in the $n=1$ LL.

$=(\hbar/eB)^{1/2}$ is the magnetic length] as observed by Kawaji et al.[14] For our devices, the QUILLS should occur first in the constriction region, due to the highest radial electric field there. Figure 8(a) shows a typical QUILLS process occurring at the local Fermi level. In the vicinity of $\nu=2$ and at a fixed V_{sd} around the current step onset, a slight decrease of the filling factor results in a wider effective tunneling barrier at the local Fermi level, and therefore in a lower tunneling rate, which decreases according to $1/\tau_{el} \propto \exp(-\alpha \Delta r^2)$ (with α as a parameter related to the scattering process and Δr as the distance between initial and final edge state for the tunneling[15,16]). Thus, with decreasing filling factor, the onset of the current step is expected to shift to a higher $|V_{sd}|$, accompanied by the step height settling on a lower value. This behavior is just as demonstrated by the data (see Figs. 4–6). The strong dependence of the tunneling rate on Δr implies a drastic influence of the steepness of the confinement potential near the trenches on the tunneling process.[17] This may explain the observed sensitivity of the formation of current plateaus to illumination, which increases the carrier density and thus the steepness of the confinement. The latter results in reduced Δr values, and hence in an increase of the tunneling rate.

Based on the above arguments, we propose a more coherent picture for our system, combining the QUILLS process and the limitation of the tunneling current by the states around the island. As schematically described in Fig. 8(b), the electrostatic potential profile between the two trench fingers and the antidot is strongly nonlinear in the QH regime.[18] The major part of the V_{sd} drop occurs near the two trench fingers at the barriers b_s and b_d, i.e., the electric field is strongest at b_s and b_d.[18] Therefore, near the onset of the current steps, the QUILLS process occurs first at the source region b_s, injecting the electrons from the compressible strips at the source region into the state of the $n=1$ LL, which are empty in case of zero V_{sd} bias. Driven by the strong radial source-drain electric field, these injected ''hot'' electrons travel diffusively under energy relaxation within the $n=1$ LL toward the island in the $n=1$ LL. At barrier b_{a1}, they relax and occupy the electron states around the island. The occupation of these island states [depicted as grey circles in Fig. 8(b)] by electrons from the $n=1$ LL is energetically favorable until all the states around the island are filled by the electrons up to the energy level of the $n=1$ LL. Due to the strong dependence of the tunneling rate according to $1/\tau_{el} \propto \exp(-\alpha \Delta r^2)$, tunneling is favorable for electrons in the energetically uppermost position, i.e., near the $n=1$ LL where the tunneling distance is the least. In the energy interval $E_F < E < E_{n=1\,LL}$, the tunneling rate to and from island states decreases drastically with energy. This means that only the uppermost populated nonequilibrium states, which are fixed at about $\hbar \omega_c/2$ above the local Fermi level, can provide a significant contribution to the tunneling current. ''Hot''-electron transport in the $n=1$ LL around the island is suppressed by cold regions separating the hot spots (see below and Fig. 9). This is the ''bottleneck'' which limits the tunneling current. The electrons tunnel further to the drain in the $n=1$ LL, and finally reach the drain, passing the barrier b_d. Thus a complete tunneling-current path forms between source and drain. In this regime, the current cannot change very much with the source-drain voltage, because most of the V_{sd} drop occurs near the edges of the two trench fingers [Fig. 8(b)]. Thus, only a weak electrostatic potential change occurs at the island, in response to the V_{sd} change across the whole constriction. The current plateau persists until the complete local breakdown of the QHE around the island is reached. In this case, the electrons populate the $n=1$ LL not only in the areas between the trenches and the island. Instead, the electrons circumvent the island in the $n=1$ LL, if their energy gain rate can balance the energy relaxation rate everywhere on their way around the island.

If the island is very small, so that the capacitance C of the island states is small enough to fulfill the condition $k_B T < E_c = e^2/2C$, Coulomb blockade effects[19] can additionally influence the tunneling. This can be important for the two samples with the smallest islands of $0.1 \times (0.25 - 0.3)$ μm^2. An estimate of the Coulomb charging energy on the basis of $E_c = e^2/2C \approx e^2 \ln(r/r_0)/8\pi^2 \epsilon \epsilon_0 r$ $(r_0 \ll r)$,[20] where $\epsilon=13$ is the dielectric constant of GaAs, yields $E_c \approx 200$ μeV, which is larger than the thermal energy $k_B T \approx 80$ μeV at $T=1$ K (with $r_0 \approx 2l_B$). The Coulomb gap would restrict the tunneling process strictly to the uppermost electron state of the island, instead of including a continuum of states (nevertheless, with a drastic suppression of the contribution of deeper states). This might explain the observed tendency of better pronounced steps with shrinking island size. However, the
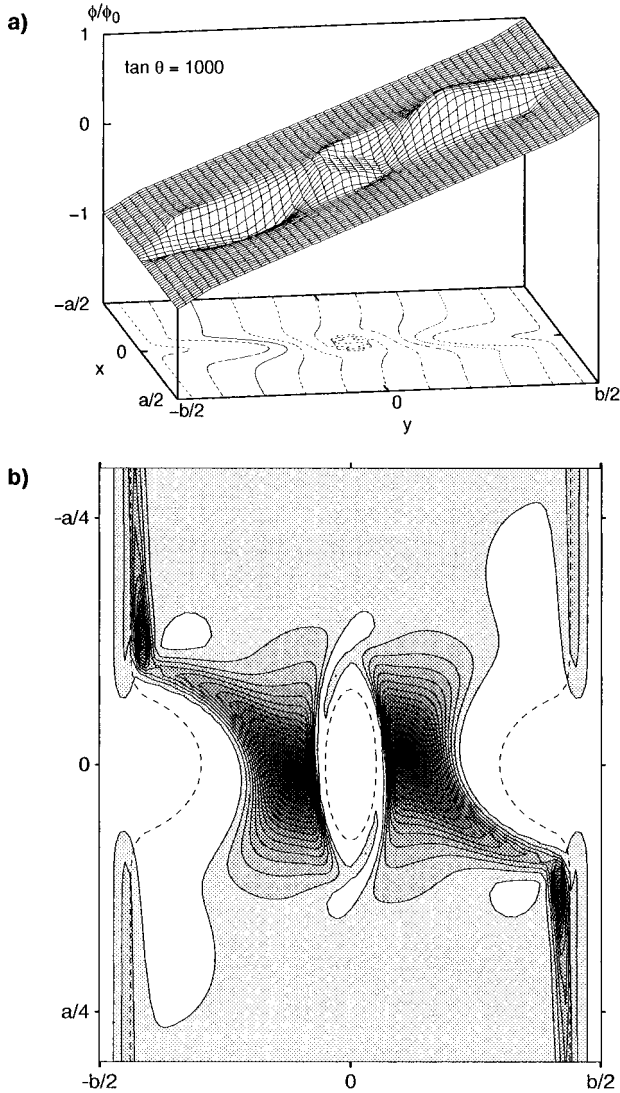
FIG. 9. (a) Electrochemical potential $\phi(x,y)$ for a current flow through the constriction described in the text, calculated from $\nabla \cdot (\hat{\sigma}[n(\mathbf{r})] \cdot \nabla \phi) = 0$. The projection shows the equipotential lines, which indicate the direction of the current density since $\sigma_{yx}/\sigma_{xx} = 10^3$. (b) Distributions of the local dissipation, corresponding to the potential profile shown in (a). Two separate hot spots (black regions) are clearly visible between each trench and the island. Dashed lines define the shape of the constriction and the island.

clear demonstration of the current step at rather large islands shows that the Coulomb blockade is not an inevitable condition for the effect.

The system can be depicted by an equivalent circuit as presented in Fig. 8(c): the QUILLS processes are represented by the four tunneling barriers marked by b_s, b_{a1}, b_{a2}, and b_d. The transport of the electrons in the $n=1$ LL between b_s and b_{a1}, and between b_{a2} and b_d are represented by resistances R_1 and R_2, respectively. All the barriers and the resistances depend on the filling factor, the V_{sd} bias and the detailed potential profile in the constriction.

To complete this qualitative picture, we have performed calculations of the distribution of the current, the potential, and the local energy dissipation inside the constriction with an antidot island. These calculations were performed within a classical model described previously,[21] which assumes a

local conductivity tensor $\sigma_{\mu\nu}[n(\mathbf{r})]$ proportional to the local electron density $n(\mathbf{r})$. To adapt the model to the present QHE situation near $\nu=2$, a Hall angle $\theta \approx 90°$, with $\tan \theta = \sigma_{yx}/\sigma_{xx} = 10^3$, is chosen. This Hall angle corresponds to the ratio $|I_c/I_{sd}|$ of the circular QH current $|I_c| = |\sigma_{xy} V_{sd}|$ and the measured tunneling current $|I_{sd}|$, which are $|I_c| \approx 4$ μA and $|I_{sd}| \approx 4$ nA, respectively.

Sample boundaries, islands, and trench fingers are modeled by a suppression of the electron density below its current bulk value n_b by Gaussian factors, producing $n(x,y) = 0$ at $y = \pm b/2$ and at $x=y=0$, and $n(\mathbf{r}) = 0.9 n_b$ along the dashed lines in Fig. 9(b). A small, but finite, value of σ_{xx}, as present under the experimental conditions, is taken into account, but nonlinear and quantum effects are neglected.

Figure 9(a) shows the electrochemical potential $\phi(\mathbf{r})$ [corresponding to the dash-dotted line in Fig. 8(b)] calculated from the continuity equation. Since $\theta \approx 90°$, the current density flows along the lines of constant $\phi(\mathbf{r})$. The related distribution of the local energy dissipation $\sigma_{xx}(\mathbf{r})[\nabla \phi(\mathbf{r})]^2$ is shown in Fig. 9(b), where regions with higher dissipation appear darker. It is interesting to note that the white regions with very low dissipation, i.e., practically vanishing current density, which surround island and trenches, reach considerably beyond the regions with substantially reduced electron density. This indicates that a more sophisticated local conductivity model would yield the same result.[21]

In Fig. 9(b), two hot spots, located between the island and the trenches, are clearly visible. These hot spots are well separated by cold regions, as we assumed for the discussion of the bottleneck limiting the tunneling current. Inside the hot spots, a stationary occupation of the $n=1$ LL by excited electrons is possible, corresponding to the tunneling resistances R_1 and R_2 of Fig. 8(c). Thus this model calculation supports our interpretation of the experimental results. However, a quantitative theory of the observed I-V curves, including a self-consistent treatment of electrostatic potential, electron density, and current density, and a treatment of nonlinear heating as well as quantum-mechanical tunneling effects, goes far beyond the scope of this model.

V. SUMMARY

In summary, we have studied the I-V characteristics at filling factors near $\nu=2$ of tunneling devices, defined in a Corbino sample by two trench fingers and a mesoscopic island. Well-developed current steps have been observed, which are attributed to a bottleneck effect of electron states around the island limiting the tunneling current. The alteration of the current steps with filling factor is explained by the shift of the Fermi energy in conjunction with quasielastic tunneling between Landau levels near the sample boundaries. An increase of the temperature and the island's size leads to a softening of the current plateaus in accordance with the physical picture suggested.

ACKNOWLEDGMENTS

[1] B. I. Halperin, Phys. Rev. B **25**, 2185 (1982).

[2] P. Středa and L. Smrčka, J. Phys. C **16**, L895 (1983).

[3] M. Büttiker, Phys. Rev. B **38**, 9375 (1988).

[4] K. v. Klitzing, G. Dorda, and M. Pepper, Phys. Rev. Lett. **45**, 494 (1980).

[5] R. J. Haug, Semicond. Sci. Technol. **8**, 131 (1993).

[6] C. J. B. Ford, P. J. Simpson, I. Zailer, D. R. Mace, M. Yosefin, M. Pepper, D. A. Ritchie, J. E. F. Frost, M. P. Grimshaw, and G. A. C. Jones, Phys. Rev. B **49**, 17 456 (1994).

[7] G. Kirczenow, A. S. Sachrajda, Y. Feng, R. P. Taylor, L. Henning, J. Wang, P. Zawadzki, and P. T. Coleridge, Phys. Rev. Lett. **72**, 2069 (1994).

[8] V. J. Goldman and B. Su, Science **267**, 1010 (1995).

[9] V. G. Burnett, A. L. Efros, and F. G. Pikus, Phys. Rev. B **48**, 14 365 (1993).

[10] G. Pilling, D. H. Cobden, P. L. McEuen, C. I. Duruöz, and J. S. Harris, Jr., Surf. Sci. **362**, 652 (1995).

[11] L. Eaves and F. W. Sheard, Semicond. Sci. Technol. **1**, 346 (1986).

[12] L. Bliek, G. Hein, V. Kose, J. Niemeyer, G. Weimann, and W. Schlapp, *High Magnetic Fields in Semiconductor Physics*, Springer Series in Solid-State Sciences, Vol. 71 (Springer, New York, 1987), p. 113.

[13] M. E. Cage, G. Marullo-Reedtz, D. Y. Yu, and C. T. van Degrift, Semicond. Sci. Technol. **5**, 351 (1990).

[14] S. Kawaji, K. Hirakawa, M. Nagata, T. Okamoto, T. Fukase, and T. Gotoh, J. Phys. Soc. Jpn. **63**, 2303 (1994).

[15] S. Martin and S. Feng, Phys. Rev. Lett. **64**, 1971 (1990).

[16] T. Ohtsuki and Y. Ono, J. Phys. Soc. Jpn. **58**, 3863 (1989).

[17] G. Müller, D. Weiss, K. v. Klitzing, K. Ploog, H. Nickel, W. Schlapp, and R. Lösch, Phys. Rev. B **46**, 4336 (1992).

[18] A. H. MacDonald, T. M. Rice, and W. F. Brinkman, Phys. Rev. B **28**, 3648 (1983).

[19] U. Meirav and E. B. Foxman, Semicond. Sci. Technol. **10**, 255 (1995).

[20] P. A. Lee, Phys. Rev. Lett. **65**, 2206 (1990).

[21] G. Nachtwei, Z. H. Liu, G. Lütjering, R. R. Gerhardts, D. Weiss, K. v. Klitzing, and K. Eberl, Phys. Rev. B **57**, 9937 (1998).